Hindawi
Advances in Materials Science and Engineering
Volume 2022, Article ID 4118048, 10 pages
https://doi.org/10.1155/2022/4118048

Research Article

Biosynthesis of Selenium Nanoparticles and Evaluation of Its Antibacterial Activity against Pseudomonas aeruginosa

Fatemeh Shakeri,[1] Fatemeh Zaboli,[1] Esmail Fattahi,[2] and Hamid Babavalian [1]

[1]*Department of Microbiology, Ayatollah Amoli Branch, Islamic Azad University, Amol, Iran*
[2]*Department of Biology, Ayatollah Amoli Branch, Islamic Azad University, Amol, Iran*

Correspondence should be addressed to Hamid Babavalian; h.babavalian@yahoo.com

Received 29 December 2021; Accepted 24 April 2022; Published 25 May 2022

Academic Editor: Alicia E. Ares

Background. A fundamental component of innate immunity is represented by skin that acts as a first aid against infection. The skin's epithelial barriers, respiratory tract, and eyes directly contacting with the external environment have incremented the probability of infection. The opportunistic pathogen *Pseudomonas aeruginosa* causes various infections in immunocompromised hosts. In addition, one-third of *P. aeruginosa* clinical isolates are resistant to three or more antibiotics. Lately, lots of researchers concentrate on halophilic microorganisms due to affordable novel biomolecules. One of these biomolecules is metal nanoparticles. MNPs exhibited antimicrobial functionality against a variety of microbes. Amidst MNPs, SeNPs are one of the most extensively studied. In this study, halophilic bacteria from solar saltern were employed for the biosynthesis of SeNPs. *Aim*. This study aimed to evaluate the antibacterial properties of SeNPs which are synthesized by halophilic microorganisms. *Result*. The NPs were synthesized by *Halomonas eurihalina* intracellularly. The produced SeNPs were identified through various assays such as UV-Vis spectroscopy, XRD, DLS, FTIR, and SEM. UV-Vis spectroscopy confirmed the presence of SeNPs. In addition, the average particle size of SeNPs was 260 nm. FTIR confirmed the presence of the capping agent to inhibit the aggregation of SeNPs. Also, synthesized selenium nanoparticles have a natural crystalline nature that is verified by XRD. SEM also revealed the spherical shape. Furthermore, SeNPs represented significant antibacterial activity against *P. aeruginosa*. *Conclusion*. According to the obtained result, biosynthesized SeNPs demonstrated remarkable characteristics that make them profitable nonantibiotics and also decrease the morbidity and mortality associated with tissue infections.

1. Introduction

Pseudomonas aeruginosa as gram-negative bacteria are found in various natural habitats since they can simply adapt to various circumstances. As a result of the ability for quick adaptation, they are identified as opportunistic pathogens [1, 2]. The opportunistic pathogen *Pseudomonas aeruginosa* causes various infections in immunocompromised hosts. The most significant infections are related to soft tissues, such as burn and chronic wounds [3]. A fundamental component of innate immunity is represented by skin acting as a first aid against infection. It activates cell-mediated and humoral immune responses [4]. Evidence indicates that *P. aeruginosa* causes epithelial damage (Evidence for Epithelial Integrity Changes by *Pseudomonas aeruginosa*). Moreover, it weakens mechanisms for post-injury epithelial repair (Evidence for Epithelial Repair Impairment by *Pseudomonas aeruginosa*). In fact, uninfected epithelia can set up an organized procedure of complex mechanisms for restoring postinjury epithelial integrity and function. Meanwhile, the capability of epithelial tissues to adequately repair is restrained by the presence of *P. aeruginosa* resulting in altered organ function and persistent infections. Several studies have presented the evidence for the negative effect of *P. aeruginosa* on repair processes and epithelial integrity in the world. In these studies, different species, pathologies, epithelia, and organs were investigated. Thus, effective postinjury repair mechanisms are vital for maintaining epithelial integrity. However, these healing procedures can be inadequate for

restoring epithelial integrity, remarkably in infectious circumstances. Since *Pseudomonas aeruginosa* infections in cutaneous and corneal principally cause disabilities, hospitalizations, and mortality in the world, they have attracted particular concerns [5]. Bacteria normally included in skin infections are P. *aeruginosa*, MRSA, Acinetobacter spp., *E. coli*, and coagulase-negative staphylococci, such as *Staphylococcus lugdunensis* and *Staphylococcus epidermidis* [4]. Different organs are infected by *Pseudomonas aeruginosa* like skin, eye, ear, heart, soft tissue, blood, or joints and bone and respiratory, gastrointestinal, urinary, as well as central nervous systems. The skin's epithelial barriers, respiratory tract, and eyes directly contacting with the external environment have incremented the probability of infection. Therefore, corneal, cutaneous, alveolar, and airway infections should be concerned about their prevalence. Mostly, the cutaneous epithelium's P. *aeruginosa* infections happen after injuries. Therefore, patients with chronic cutaneous wounds and burn victims, a prevalent complication of diabetes, are mainly at higher risks of developing *P. aeruginosa* infections [1, 5]. In addition, one-third of *P. aeruginosa* clinical isolates are resistant to three or more antibiotics, including third-generation cephalosporins and imipenem, which have been the gold standard antibiotics for *P. aeruginosa* infection [6, 7].

Nanotechnology focuses on the employment of molecular and atomic techniques to arrange materials at a nanoscale with remarkable physical, chemical, and biological properties [8]. Nanotechnology has a wide variety of applications such as food, electronics, pharmaceuticals, fuels, chemicals, polymers, and environmental health [9]. Nanoparticles pose high reactivity due to the high surface, small size, and surface chemistry [10, 11]. In addition, as a result of significant antibacterial effect and low toxicity on human cells of metal nanoparticles (MNPs) like silver (Ag), cerium (Ce), iron (Fe), selenium (Se), silicon (Si), titanium (Ti), and zinc (Zn), they attracted special attention [11–13]. Also, MNPs exhibited antimicrobial functionality against a variety of microbes [11, 13]. Amidst MNPs, SeNPs are one of the most extensively studied [14]. Se gains a special palace in the field of medicine [15]. Se incorporated in the structure of several enzymes like glutathione peroxidases (GPx), iodothyronine deiodinases, and thioredoxin reductase (TrxR) that play role in the process like antioxidation, detoxification, and metabolism [8, 15–17]. Various forms of selenium oxyanions such as selenide (SeII), selenite (SeIV), or selenate (SeVI) have toxicity on animals as well as human cell lines while the elemental form of selenium (SeO) under biological concentration (<400 μg/mL) did not show toxicity. Also, selenium exists in either organic form like selenocysteine (Secys) and selenomethionine (Semet) or inorganic form including selenate (SeO_4^{2-}), selenide (Se^{2-}), and selenite (SeO_3^{2-}) [18]. SeNPs demonstrated remarkable antimicrobial activity against *Candida albicans* [19], *Streptococcus mutans* [20], *Staphylococcus aureus* [21, 22]. Moreover, the biological characteristics of SeNPs including antibacterial, antiviral, and antioxidant activity that possess low toxicity on human cells have presented an area for research in nanotechnology [8, 14].

Various physiochemical methods have been applied to synthesize SeNPs [16]. On the other hand, the synthesis of NPs by employing microorganisms and plants provides new, clean, safe, and eco-friendly techniques [8, 10, 17, 23]. Furthermore, the biosynthesized NPs generally capped via cellular metabolites that are related to the microorganisms [9, 24].

Different bacteria in the aquatic environments as well as terrestrial, either in selenium-rich or selenium-free soils, have the capability to reduce selenite/selenate oxyanions. As a result of the continuous introduction of industrial and urban swage, halophilic microorganisms face toxic metals, including Se which result in enduring toxic ions and changing them to wither less poisonous or nanoparticles [18, 25, 26]. Although the potential of salt-tolerant bacteria for reduction of selenite or selenate and other anions in high salt concentrations has been relatively less explored [16], existing in these severe environments like high-salt concentration needs cell components that make them typical microorganisms [9]. Lately, lots of researchers concentrate on halophilic microorganisms due to afford novel biomolecules [27]. Therefore, halophilic microorganisms have the capacity to be applied in biotechnological procedures including biopolymers, hydrolytic enzymes, biosurfactants, biofuels, and bioremediation [9]. Therefore, this study aimed to employ halophilic strain to synthesize SeNPs and determine their antibacterial properties on *P. aeruginosa*.

2. Material and Methods

2.1. Materials. Sodium Selenite was purchased from Sigma Aldrich. All other chemicals used in this study were of analytic grade.

2.2. Isolation and Characterization of the Bacterial Strains

2.2.1. Pseudomonas aeruginosa. In this study, 2 different strains of *P. aeruginosa* were used. These strains are *P. aeruginosa* ATCC 9027 and *P. aeruginosa* isolated from ulcers. Strains obtained from the University of Tehran have been molecularly identified.

For the PCR method, the primers were 9F and 1541R, and their sequences have been shown in Table 1. In addition, BLAST was performed via NCBI data bank.

2.3. Halophilic Bacteria

2.3.1. Isolation. The halophilic microorganism was isolated from Hoz-e Soltan area which is a salt lake located in Qom, Iran. In addition, to culture halophilic bacteria, salt water 10% (SW) is used.

2.3.2. DNA Extraction. In the first stage of extraction, remove some of the colony and add it to 200 μl of Tris-ethylene diamine tetra acetic acid buffer and then vortex it to dissolve completely. The contents of this buffer cause DNA to separate and also act as a chelator, leading to the loosening

Table 1: Primers sequencing was used for PCR assay to characterize the strains that isolated from wounds.

Primers	Sequence
9F	5′-AAG AGT TTG ATC ATG GCT CAG-3′
1541R	5′-AAG GAG GTG ATC CAG CCG CA-3′

of the wall. In the second step, 20 μl of 1 mg/ml lysozyme was added and incubated for 37 minutes at 37°C. This lysozyme breaks down the bacterial wall. In the third step, 100 μl of 1% SDS solution is added and reheated in the incubator for 30 minutes to dissolve the fat in the cell wall and eliminate it. In the fourth step, add 100 μl of 5 mM NaCl and leave the solution at 65°C for 30 minutes. Salt breaks down DNA-bound proteins more easily. In the fifth step, the same volume of chloroform solution was added and the solution was centrifuged at 11500 rpm for 15 minutes to form 3 layers. Separate the supernatant or top layer. The fifth step is performed three times, and in the sixth step, isopropanol (cold isopropanol) is added to the solution and refrigerated for 24 hours. In the seventh step, after 24 hours, centrifuge at 11500 rpm for 15 minutes and then remove the supernatant. In the eighth step, 70% ethanol is used, which is added in the amount of 200–300 microns per liter, dissolved in ethanol using blows, and in the next step, for 15 minutes centrifuge at 11500 rpm. In the tenth step, discard the topical solution, which was ethanol, so that no ethanol remains in the vial. In the last step, 200 microliters of TE buffer were used to store the extracted DNA.

2.3.3. PCR. To perform PCR on the DNA extracted in a vial, we add the materials in Table 2 in order and place them in the PCR machine. It is also a DNA-free vial, which we test as a negative control. The primers used with the desired sequences are also listed in Table 3.

2.3.4. 16srRNA Sequencing. The sample was sent to the Pishgam Company along with the 16SrRNA primer for sequencing. After sequencing the amplified fragment of the 16SrRNA gene, the isolated strain was compared with other sequences in the gene bank at the NCBI site using Blast software [28].

2.3.5. Phylogenic Tree. In this section, the similarity of the desired strain with similar strains was first obtained. For this purpose, the sequence edited by ChromasPro software is compared with the sequences registered in NCBI and EZTAXON databases. The sequence was then saved in the desired FASTA format to draw the phylogenetic tree. In the next steps, phylogenetic analysis of the desired strain and similar strains was performed using Mega7 software. Maximum liquidity method was also used to draw the phylogenetic tree of this strain. The validity of the branches in the drawn tree was checked using bootstrap analysis algorithm and sampled 1000 times.

Table 2: Materials required for PCR.

Materials	Amount (total volume = 30μ)
DDW	12
Forward primer	1
Reverse primer	1
Extracted DNA	1
Master mix	15

Table 3: Primers sequencing to employ for PCR experiments to characterize halophilic strain.

Primers	Sequencing
27F	5′-AGAGTTTGATCCTGGCTCAG-3′
1492R	5′-GGTTACCTTGTTACGACTT-3′

2.4. Biosynthesis of SeNPs

2.4.1. Intracellular. For intracellular synthesis, 200 ml of SW10% was inoculated with the isolated strain and sodium selenite (final concentration of 5 mM) which was filtrated through 0.2-micron filters. The mixture was incubated at 40°C for 24 hours. Simultaneously, uninoculated SW10% with sodium selenite was employed as a control [9].

2.4.2. Extracellular. For this method, the bacterium was first inoculated in 200 ml of sterile SW10% culture medium and then incubated at 150 rpm for 48 hours in an incubator shaker. In the second step, the inoculated culture medium was centrifuged at 4000 rpm for 20 minutes, and the supernatant was separated. The obtained supernatant was then passed through a 0.22-micron filter, and in the next step, 5 mM filtered sodium selenite was added to it. The mixture was placed in an autoclave for 20 minutes at a pressure of 1 atmosphere at 121°C [9].

2.5. Purification of SeNPs. To purify SeNPs, the bacterial cells were harvested by centrifuge at 4000 rpm for 20 minutes. Then, the lysis buffer (SDS1% and lysozyme) was added to the harvested cells. In addition, this mixture is sonicated for 20 minutes. 1-Octanol was added to this mixture and incubated overnight at 4°C. Sediments were collected and washed through chloroform, absolute ethanol, ethanol 70%, and distilled water, respectively [9].

2.6. Characterization of SeNPs

2.6.1. Visual Observation. Changing the yellow color of the culture media through visual observation confirmed the generation of SeNPs [9].

2.6.2. UV-Visible Spectroscopy. SeNPs were dissolved in distilled water through sonication (20 min, 110 W). 1 mL of dispersed NPs was added to the covet. Then, the absorbance of SeNPs between 200 and 800 nm was noted by Shimadzu

UV-1601, and also for the blank, distilled water is used. In addition, sodium selenite dissolved in water is used as a control [9].

2.6.3. Dynamic Light Scattering (DLS). 1 mL of dissolved SeNPs in water was sent to the Central Laboratory at Tehran University for measuring the particle size and distribution with utilizing HORIBA.

2.6.4. X-Ray Diffraction (XRD). This assay determined crystal shape of SeNPs [9]. Radiation source was recorded by the XRD method (40 kV/40 mA, 10° to 80°, a step size of 0.04 of seconds) [29].

2.6.5. Fourier Transform Infrared Spectroscopy (FTIR). To identify functional chemical groups on the exterior area of SeNPs [9], this assay was performed. The sample was tested using Tensor 27 via KBr pellet method as described by Nakamoto [30] in the range of 400–4000 cm^{-1} at a resolution of 4 cm^{-1} [9].

2.6.6. Scanning Electron Microscopy. The SeNPs were fixed and stabilized for 2 hours in 2% of glutaraldehyde at 27°C, then it is dehydrated, and also coated with gold. The fixed SeNPs were observed via MIRA3 to identify the morphological characteristics of SeNPs [31].

2.7. Antibacterial Activity

2.7.1. Well Diffusion Assay. Two wells on the culture medium were produced by pipet Pasteur. Then, new culture of bacteria was prepared by Sterile swab. 0.0932 gr of SeNPs was dispersed in a 500 mL water. 100 μ of final concentration was loaded in one of the wells. For the second well that is considered as a standard well, 100 μ of culture media without bacteria and SeNPs were added.

2.7.2. Antibiotic Susceptibility. Susceptibility of isolated and standard strains to the antibiotic including Clindamycin, Nitrocefin, Sulfadiazine/trimethoprim, Sulphamethoxazole/trimethoprim, Ampicillin/sulbactam, Temocillin, Penicillin, Ceftazidime, Amphotericin B, Gentamicin, Ciprofloxacin, Pipemidic acid/tazobactam, Co-trimoxazole, Amikacin, Imipenem, Tetracycline, and Lincomycin was evaluated via the disk diffusion approach according to the Clinical and Laboratory Standards Institute (CLSI). To perform this experiment, a new culture of the strain was prepared, and antibiotic disks were added to each plate and incubated for 24 hours at 30oC.

3. Result

3.1. Characterization of Isolated Strains

3.1.1. Pseudomonas aeruginosa. Microscopic observation represented gram-negative and bacillus morphology of the strain. In addition, the result of the molecular assay has been presented in the table below (Table 4).

3.2. Halophilic Bacteria

3.2.1. 16SrRNA Sequencing. The result demonstrated that the isolated strain showed 98/30% similarity to the *Halomonas eurihalina*. This is the first report on the biosynthesis of SeNPs by *H. eurihalina*. In addition, the result has been shown in Table 5.

3.2.2. Phylogenic Tree. Moreover, with the sequence, the phylogenic tree was conducted via MEGA 7 which is shown in Figure 1.

3.2.3. Biosynthesis of SeNPs. This halophilic strain is able to produce the SeNPs via intracellular approach. In the succeeding parts, biosynthesized SeNPs were prepared for further analysis.

3.3. Characterization of SeNPs

3.3.1. Visual Observation. Color transition of culture media from to brick-red represented the formation of SeNPs which is shown in Figure 2.

3.3.2. UV-Visible Spectroscopy. For the primary confirmation, UV-Vis spectrophotometry was conducted. The sharp absorption peak has been seen at 275 nm that is possibly associated with the surface plasmon vibrations. However, no sharp peak is seen for the control sample (Figure 3).

3.3.3. Dynamic Light Scattering (DLS). Biosynthesized NPs size was within 200–400 nm, and also, the average size (Z-average) was 260 nm. Moreover, the polydispersity index was 0.2 (Figure 4).

3.3.4. X-Ray Diffraction (XRD). In Figure 5, on the 2θ axis of the diagram, there has been 5 peaks that belong to the 23.2°, 29.5°, 45.5°, 55.5°, and 59.8° corresponding to the (100), (101), (111), (113), and (202). In addition, this assay represented great peaks all over the whole spectrum ranging 20 to 80.

3.3.5. Fourier Transform Infrared Spectroscopy (FTIR). The first and second peaks, which are between 626.21 and 681.88 cm^{-1}, are related to C-Cl bond vibration. The third peak with wavelength cm^{-1} is 865.61 related to C-O. The fourth peak with wavelength cm^{-1} is 996.92, and the other peak with wavelength cm^{-1} is 1393.16 due to the presence of C-H bond. The 1637.60 cm^{-1} wavelength corresponding to the sixth peak is the first type of hope due to the presence of carbonyl amide bonds of proteins. The wavelength of 2175.12 cm^{-1}, which is the seventh peak, is due to the vibrations of alkynes (carbon-carbon triple bond). Also, the eighth peak with a wavelength of 2917.78 cm^{-1} is associated

Table 4: Different properties of wound strain.

Strain name	Sequence length	Microorganism	Accessibility code	Similarity
Wound sp.	739	*Pseudomonas aeruginosa* MLTBM2	MT646431.1	99/19

Table 5: Different properties of characterized halophilic strain.

Strain name	Sequence length	Microorganism	Accessibility code	Similarity
H98	780	*Halomonas eurihalina*	L42620	98/30

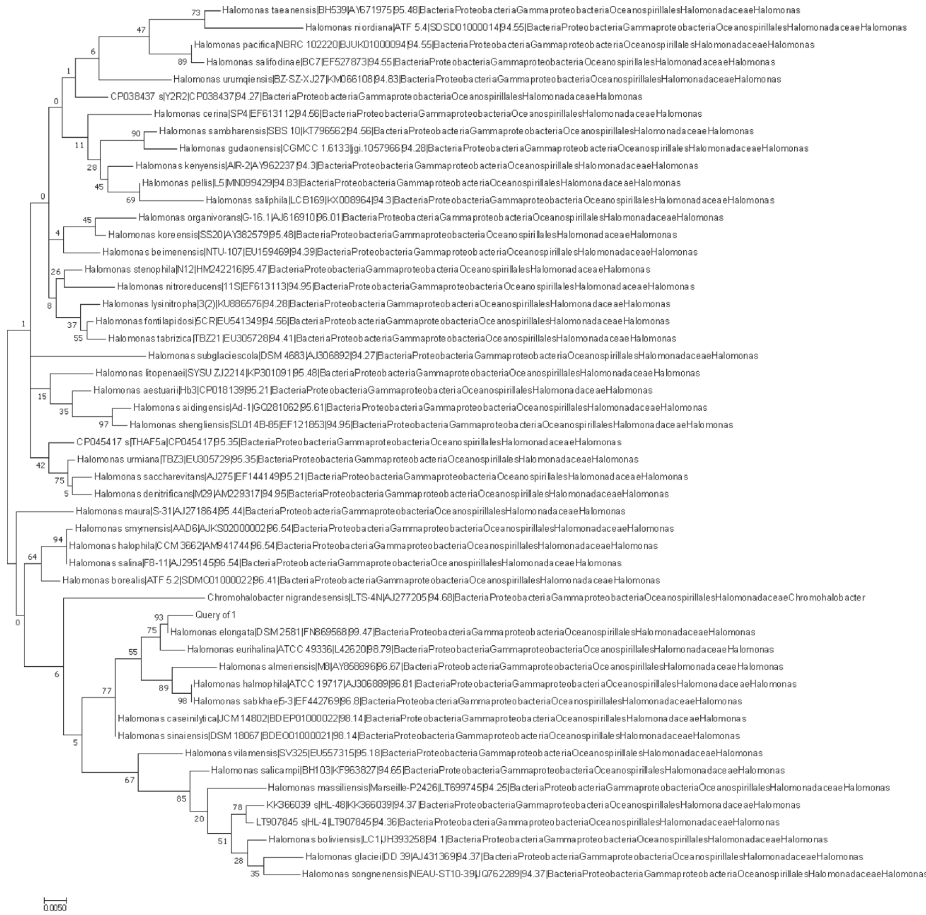

Figure 1: Phylogenic tree conducted by MEGA7. Query 1 represented the isolated strain that is the most similar to *Halomonas eurihalina*.

with asymmetric tensile vibrations of the C-H groups. The last peak related to the wavelength 3237.12 cm^{-1} which can be related to the O-H groups. These moieties inhibit the aggregation of SeNPs and make them more stable. All results have been shown in Figure 6.

3.3.6. Scanning Electron Microscopy. The results showed the dispersion of particles in size and also show that the biosynthetic nanoparticles have spherical surface (Figure 7).

3.3.7. Well Diffusion. The result showed 2.5 cm inhibitory zone diameter for standard strain and 2 cm for a strain isolated from wound. Also, the obtained results have been represented in the picture below (Figure 8).

3.3.8. Antibiotic Susceptibility. Based on susceptibility to disks, strains were divided into two groups sensitive and resistant. In this study, collected strains that were isolated of wounds and urinary were resistant to all types of antibiotic disks. In addition, respiratory strains were sensitive to Amikacin and Pipemidic acid/tazobactam and resistant to the other antibiotics, and also, the standard strain was sensitive to Co-trimoxazole, Amikacin, Temocillin, and Pipemidic acid/tazobactam. Table 6 demonstrates the results.

4. Discussion

The complication of a bacterial infection within the burn wound is one of the highest challenges in the burn clinic. It may result in more severe disease states such as sepsis. The

Figure 2: Conversion of Selenium to elemental Selenium.

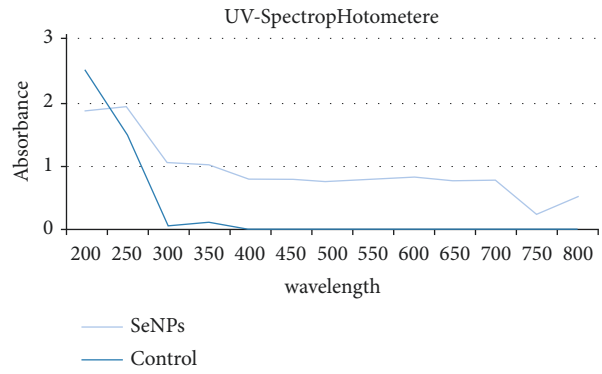

Figure 3: Control sample has not shown any absorption changes while at 275 nm SeNPs showed sharp peak.

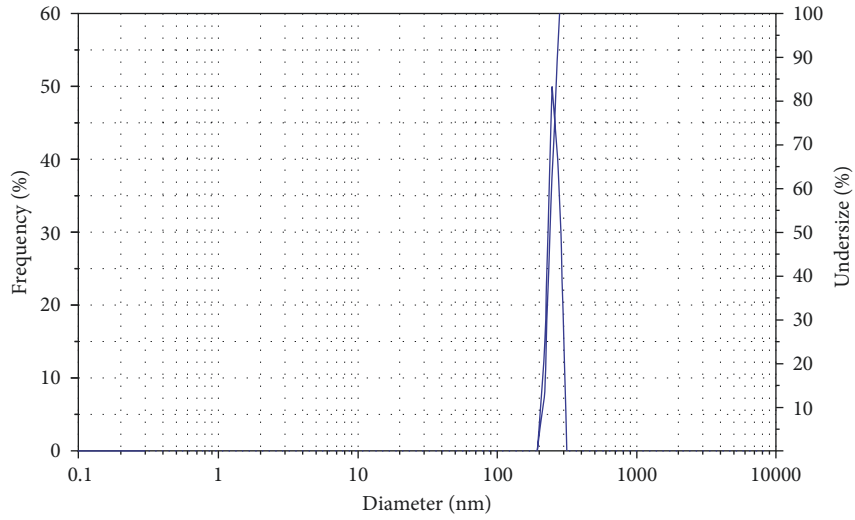

Figure 4: This picture shows the particles' size and distribution that 63% of NPs were 240 ± 49.

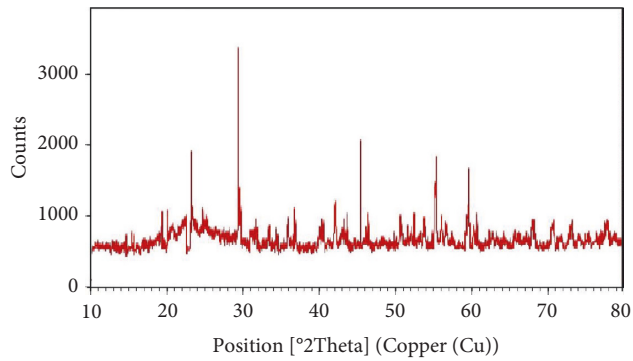

Figure 5: The results represented the crystalline nature of biosynthetic nanoparticles.

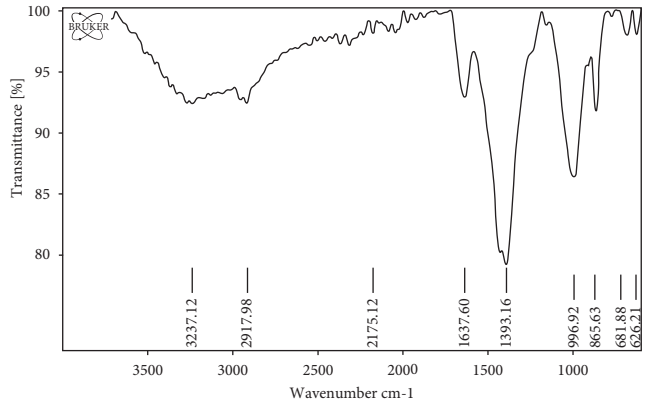

Figure 6: This chart is related to the results of FTIR test. The chart shows 9 peaks. Each of these peaks with the indicated wavelengths belongs to specific functional groups that have been involved in the synthesis or are known as nanoparticle stabilizers.

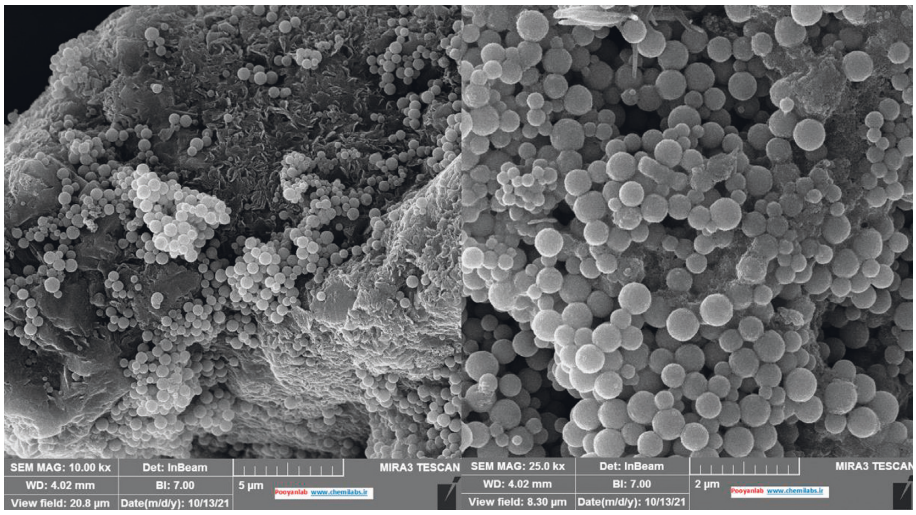

(a) (b)

Figure 7: SEM analysis results. (a) The right figure is with a magnification of 10,000; (b) The left figure is a biosynthetic nanoparticle with a magnification of 25,000.

challenge imposed by resistant microorganisms is further escalated by the scarcity of new antimicrobials, particularly antibiofilm agents in the treatment of burn wound infections. Various animal models are used for recapitulating the hallmarks of clinical burn wound infection and assisting to develop new antimicrobial treatments. The pigs, rats, and mice are the three most common models of burn wound infection *in vivo*. The best substitute for human skin is the porcine model. However, high costs and ethical implications hinder their usages for screening vast libraries of

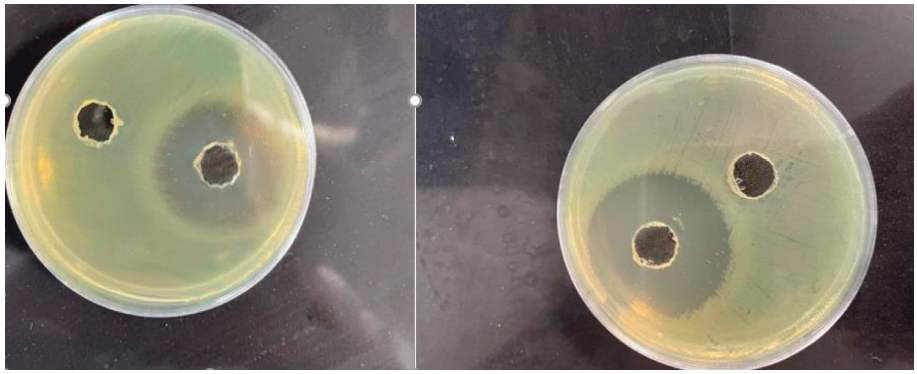

(a) (b)

Figure 8: (a) Standard strain (left picture) showed more susceptibility to biosynthesized SeNPs; (b) also, the right picture is isolated strain.

antimicrobials. Mice present the highest range of advantages to characterize aspects of the host's reaction to burn infection, in terms of genetic mutants. However, they are often restricted to acute (less than 48 h postinoculation) burn wound infection prior to the fast onset of sepsis and death, possibly owing to requiring for injecting the higher bacterial inoculums under the burn eschar for inducing the burn infection. Formulating the pathogens in a biopolymer matrix is also included for driving the infection to a more chronic biofilm-like state [32].

Several studies demonstrated that the cells at the wound edges of injured airway epithelia and the denuded basement membranes are more susceptible to binding by *P. aeruginosa*. More specifically, it has been shown that *P. aeruginosa* adheres more frequently to mucus and extruded/dead cells as well as basal and migrating flattened cells with lamellipodia. Amino-acid sensor-driven chemotaxis and flagella-driven swimming appear to be the mechanisms by which *P. aeruginosa* reaches the cells at the wound edge of airway epithelia. Finally, fibronectin, asialoGM1, and $\alpha 5\beta 1$integrin may mediate *P. aeruginosa* binding to the airway epithelial cells [5].

According to the results obtained from molecular identification of 16SrRNA sequence, the obtained strain is 98/30% of *H. eurihalina*, which is isolated from Lut desert and also has the ability to biosynthesize selenium nanoparticles intracellularly.

To confirm the synthesis of nanoparticles, first, qualitatively by changing the color of the culture medium from yellow to red brick color, which is due to the conversion of selenite to selenium as an element, over time, the sodium selenite in the culture medium changes color to red [15, 23]. This indicates the reduction of selenite to elemental selenium, and also, the distinct red color created indicates the resonance of the surface plasmons of selenium nanoparticles. Slightly, the maximum light absorption was at 250 nm. In a study conducted by Dr. Mohammad Amoozgar and colleagues, the light absorption of selenium nanoparticles in the UV-Vis method was 294 nm [18]. In another paper, a group of scientists synthesized selenium nanoparticles by microorganisms isolated from different parts of Saudi Arabia, with the selected strain having an absorption peak of 290 nm [33]. Another experiment was performed in 2015 on the synthesis of selenium nanoparticles by the bacterium Ralstonia eutropha. The absorption peak for this synthetic nanoparticle is shown at 270 nm [34]. Various studies prove the resonance peak of synthetic selenium nanoparticles around 200–300 nm. However, this absorption peak also depends on various factors such as particle size, shape, material composition, and isolated environment of the desired strain [35]. In addition, there is a great deal of research on the formation of selenium nanoparticles, which indicates different absorption peaks for the presence of selenium nanoparticles [36].

The size of biosynthetic nanoparticles measured by the DLS test in this experiment was 260 nm on average, and the amplitude of the absorption peak in UV-Vis test also proves the dispersion of nanoparticle size. In addition, the dispersion index or PI was 0.2. In another experiment performed by Srivastava et al. on the synthesis of selenium

Table 6: Susceptibility of standard strain and wound strain to various antibiotic disks.

ATCC 9027	Wound sp.	
R	R	NI300
R	R	SAM20
R	R	IMI10
R	R	CIPR5
S	R	CTR30
S	R	TEM30
R	R	TS25
S	NT	AK30
R	R	GM10
S	R	PI + TZ
R	R	SXT
R	R	AMB
R	R	CAZ
R	R	P
R	R	DA
R	R	L
S	R	TE

Ni300: nitrocefin; SAM20: ampicillin/sulbactam; IMI10: imipenem; CIPR5: ciprofloxacin; CTR30: co-trimoxazole; TEM30: Temocillin; TS25: sulfadiazine/trimethoprim; AK30: amikacin GM10: gentamicin; PI + TZ: piperacillin/tazobactam; SXT: sulphamethoxazole/trimethoprim; AMB: amphotericin B; CAZ: ceftazidime; P: penicillin; DA: clindamycin; L: lincomycin; TE: tetracycline (R: resistance; S: sensitive; NT: not tested).

nanoparticles by a bacterium, the average particle size was 70.9 nm [34]. Another experiment synthesizing selenium nanoparticles from a bacterial source showed that the particles were 170–160 nm in size [37]. It has been proven that when the scattering indices are less than 0.5, the nanoparticle stability is higher and the nanoparticle aggregation rate is lower [38].

In addition, according to research, selenium nanoparticles synthesized by bacteria are coated by various biomolecules or macromolecules such as proteins and polysaccharides. In fact, the reduction of metal salts to metal nanoparticles can be caused by carbohydrates and proteins. FTIR analysis can provide useful semiquantitative results in relation to the presence of biological compounds in the nanoparticle coating layers and their associated contents by the vibration of the functional groups (proteins and carbohydrates) of the nanoparticles [39]. The test results prove the presence of proteins and polysaccharides.

According to the results of the XRD experiment, the synthesized selenium nanoparticles have a natural crystalline nature. In another study, XRD results show that synthetic selenium nanoparticles are crystalline, which is a natural form [40]. However, in other experiments, the results showed that the synthetic selenium nanoparticles did not have any specific crystalline form, and amorph was seen [28, 41].

In addition, based on the results of the SEM test, synthetic nanoparticles are dispersed in size. This dispersion may be due to the accumulation of nanoparticles. Also, based on the morphology shown in the results, it is observed that the obtained particles have a spherical surface. In an experiment conducted by a group of researchers in 2018, synthetic selenium nanoparticles also had a spherical shape [28, 41]. In 2016, the results of SEM analysis also showed that the biosynthetic SeNPs by *P. aeruginosa* have a spherical surface [42].

5. Conclusion

Regarding the result of various analyses, it is concluded the biosynthetic SeNPs by halophilic bacteria represented suitable characteristics which possess antibacterial properties against the most common pathogenic bacteria. Hence, it is concluded that biosynthetic SeNPs can be considered as an alternative candidate for traditional antibiotics to lessen the side effect of employing antibiotics and also increasing the efficiency of therapeutics. On the other hand, further analysis and in vivo tests are in demand to find out the various aspects of employing these NPs.

Data Availability

All the data generated or analyzed during this study are included in this published article, and also, the data sets analyzed to support the findings of this study are available from the corresponding author upon request.

Conflicts of Interest

The authors declare that they have no conflicts of interest.

References

[1] V. Krylov, O. Shaburova, S. Krylov, and E. Pleteneva, "A genetic approach to the development of new therapeutic phages to fight *Pseudomonas aeruginosa* in wound infections," *Viruses*, vol. 5, no. 1, pp. 15–53, 2012.

[2] D. P. Nichols, S. Caceres, L. Caverly et al., "Effects of azithromycin in *Pseudomonas aeruginosa* burn wound infection," *Journal of Surgical Research*, vol. 183, no. 2, pp. 767–776, 2013.

[3] K. H. Turner, J. Everett, U. Trivedi, K. P. Rumbaugh, and M. Whiteley, "Requirements for *Pseudomonas aeruginosa* acute burn and chronic surgical wound infection," *PLoS Genetics*, vol. 10, no. 7, Article ID e1004518, 2014.

[4] R. Serra, R. Grande, L. Butrico et al., "Chronic wound infections: the role of *Pseudomonas aeruginosa* and *Staphylococcus aureus*," *Expert Review of Anti-infective Therapy*, vol. 13, no. 5, pp. 605–613, 2015.

[5] M. Ruffin and E. Brochiero, "Repair process impairment by *Pseudomonas aeruginosa* in epithelial tissues: major features and potential therapeutic avenues," *Frontiers in Cellular and Infection Microbiology*, vol. 9, p. 182, 2019.

[6] Z. Pang, R. Raudonis, B. R. Glick, T.-J. Lin, and Z. Cheng, "Antibiotic resistance in *Pseudomonas aeruginosa*: mechanisms and alternative therapeutic strategies," *Biotechnology Advances*, vol. 37, no. 1, pp. 177–192, 2019.

[7] S. DeLeon, A. Clinton, H. Fowler, J. Everett, A. R. Horswill, and K. P. Rumbaugh, "Synergistic interactions of *Pseudomonas aeruginosa* and *Staphylococcus aureus* in an in vitro wound model," *Infection and Immunity*, vol. 82, no. 11, pp. 4718–4728, 2014.

[8] M. Shakibaie, H. Forootanfar, Y. Golkari, T. Mohammadi-Khorsand, and M. R. Shakibaie, "Anti-biofilm activity of biogenic selenium nanoparticles and selenium dioxide against clinical isolates of *Staphylococcus aureus*, *Pseudomonas aeruginosa*, and *Proteus mirabilis*," *Journal of Trace Elements in Medicine & Biology*, vol. 29, pp. 235–241, 2015.

[9] M. Abdollahnia, A. Makhdoumi, M. Mashreghi, and H. Eshghi, "Exploring the potentials of halophilic prokaryotes from a solar saltern for synthesizing nanoparticles: the case of silver and selenium," *PLoS One*, vol. 15, no. 3, p. e0229886, Article ID e0229886, 2020.

[10] D. Medina Cruz, G. Mi, and T. J. Webster, "Synthesis and characterization of biogenic selenium nanoparticles with antimicrobial properties made byStaphylococcus aureus, methicillin-resistantStaphylococcus aureus(MRSA),*Escherichia coli*,andPseudomonas aeruginosa," *Journal of Biomedical Materials Research Part A*, vol. 106, no. 5, pp. 1400–1412, 2018.

[11] W. Majeed, M. Zafar, A. Bhatti, and P. John, "Therapeutic potential of selenium nanoparticles," *Journal of Nanomedicine & Nanotechnology*, vol. 09, no. 01, p. 2, 2018.

[12] X. Huang, X. Chen, Q. Chen, Q. Yu, D. Sun, and J. Liu, "Investigation of functional selenium nanoparticles as potent antimicrobial agents against superbugs," *Acta Biomaterialia*, vol. 30, pp. 397–407, 2016.

[13] M. Barsainya and D. Pratap Singh, "Green synthesis of zinc oxide nanoparticles by *Pseudomonas aeruginosa* and their broad-spectrum antimicrobial effects," *Journal of Pure and Applied Microbiology*, vol. 12, no. 4, pp. 2123–2134, 2018.

[14] N. S. Dumore and M. Mukhopadhyay, "Antioxidant properties of aqueous selenium nanoparticles (ASeNPs) and its catalysts activity for 1, 1-diphenyl-2-picrylhydrazyl (DPPH)

reduction," *Journal of Molecular Structure*, vol. 1205, p. 127637, 2020.

[15] H. S. Abbas, D. H. Abou Baker, and E. A. Ahmed, "Cytotoxicity and antimicrobial efficiency of selenium nanoparticles biosynthesized by Spirulina platensis," *Archives of Microbiology*, vol. 203, no. 2, pp. 523–532, 2021.

[16] B. Fardsadegh, H. Vaghari, R. Mohammad-Jafari, Y. Najian, and H. Jafarizadeh-Malmiri, "Biosynthesis, characterization and antimicrobial activities assessment of fabricated selenium nanoparticles using Pelargonium zonale leaf extract," *Green Processing and Synthesis*, vol. 8, no. 1, pp. 191–198, 2019.

[17] S. Rajeshkumar, M. Tharani, and P. Sivaperumal, "Green synthesis of selenium nanoparticles using black tea (camellia sinensis) and its antioxidant and antimicrobial activity," *Journal of Complementary Medicine Research*, vol. 11, no. 5, pp. 75–82, 2020.

[18] M. Tabibi, S. S. Agaei, M. A. Amoozegar, R. Nazari, and M. R. Zolfaghari, "Antibacterial, antioxidant, and anticancer activities of biosynthesized selenium nanoparticles using two indigenous halophilic bacteria," *Archives of Hygiene Sciences*, vol. 9, no. 4, pp. 275–286, 2020.

[19] E. Kheradmand, F. Rafii, M. H. Yazdi, A. A. Sepahi, A. R. Shahverdi, and M. R. Oveisi, "The antimicrobial effects of selenium nanoparticle-enriched probiotics and their fermented broth against Candida albicans," *Daru Journal of Pharmaceutical Sciences*, vol. 22, no. 1, pp. 48–56, 2014.

[20] G. Dhanraj, S. Rajeshkumar, and A. Omri, "Anticariogenic effect of selenium nanoparticles synthesized using *Brassica oleracea*," *Journal of Nanomaterials*, vol. 2021, pp. 1–9, 2021.

[21] P. A. Tran and T. J. Webster, "Antimicrobial selenium nanoparticle coatings on polymeric medical devices," *Nanotechnology*, vol. 24, no. 15, p. 155101, 2013.

[22] T. H. D. Nguyen, B. Vardhanabhuti, M. Lin, and A. Mustapha, "Antibacterial properties of selenium nanoparticles and their toxicity to Caco-2 cells," *Food Control*, vol. 77, pp. 17–24, 2017.

[23] K. S. Prasad, J. V. Vaghasiya, S. S. Soni et al., "Microbial selenium nanoparticles (SeNPs) and their application as a sensitive hydrogen peroxide biosensor," *Applied Biochemistry and Biotechnology*, vol. 177, no. 6, pp. 1386–1393, 2015.

[24] P. Srivastava and M. Kowshik, "Anti-neoplastic selenium nanoparticles from Idiomarina sp. PR58-8," *Enzyme and Microbial Technology*, vol. 95, pp. 192–200, 2016.

[25] P. Srivastava and M. Kowshik, *Biosynthesis of Nanoparticles from Halophiles. Halophiles. Sustainable Development and Biodiversity*, pp. 145–159, Springer, Cham, 2015.

[26] S. Tiquia-Arashiro and D. Rodrigues, *Halophiles in Nanotechnology. Extremophiles: Applications in Nanotechnology*, pp. 53–88, Springer International Publishingp, New York, NY, USA, 2016.

[27] L. Daoud and M. Ben Ali, "Halophilic microorganisms: interesting group of extremophiles with important applications in biotechnology and environment," *Physiological and Biotechnological Aspects of Extremophiles*, pp. 51–64, 2020.

[28] M. Shakibaie, M. Jafari, A. Ameri, H. Rahimi, and H. Forootanfar, "Biosynthesis and physicochemical characterization, and cytotoxic evaluation of selenium nanoparticles produced by *streptomyces lavendulae FSHJ9* against MCF-7 cell line," *Journal of Rafsanjan University of Medical Sciences*, vol. 17, no. 7, 2018.

[29] B. El-Deeb, A. Al-Talhi, N. Mostafa, and R. Abou-assy, "Biological synthesis and structural characterization of selenium nanoparticles and assessment of their antimicrobial properties," *American Academic Scientific Research Journal for Engineering, Technology, and Sciences*, vol. 45, no. 1, pp. 135–170, 2018.

[30] K. Nakamoto, *Infrared and Raman Spectra of Inorganic and Coordination Com-Pounds*, Wiley Online Library, Hoboken, New Jersey, United States, 2008.

[31] K. Kalishwaralal, S. Jeyabharathi, K. Sundar, and A. Muthukumaran, "A novel one-pot green synthesis of selenium nanoparticles and evaluation of its toxicity in zebrafish embryos," *Artificial Cells, Nanomedicine, and Biotechnology*, vol. 44, no. 2, pp. 471–477, 2016.

[32] K. S. Brandenburg, A. J. Weaver Jr., S. L. R. Karna et al., "formation of *Pseudomonas aeruginosa* biofilms in full-thickness scald burn wounds in rats," *Scientific Reports*, vol. 9, no. 1, Article ID 13627, 2019.

[33] B. El-Deeb, A. Al-Talhi, N. Mostafa, and R. Abou-assy, "Biological synthesis and structural characterization of selenium nanoparticles and assessment of their antimicrobial properties," *American Scientific Research Journal for Engineering, Technology, and Sciences (ASRJETS)*, vol. 45, no. 1, pp. 135–170, 2018.

[34] N. Srivastava and M. Mukhopadhyay, "Green synthesis and structural characterization of selenium nanoparticles and assessment of their antimicrobial property," *Bioprocess and Biosystems Engineering*, vol. 38, no. 9, pp. 1723–1730, 2015.

[35] M. Joshi, A. Bhattacharyya, and S. W. Ali, "Characterization techniques for nanotechnology applications in textiles," *IJFTR*, vol. 33, no. 3, 2008.

[36] T. Hemalatha, G. Krithiga, B. Santhosh Kumar, and T. P. Sastry, "Preparation and characterization of hydroxyapatite-coated selenium nanoparticles and their interaction with osteosarcoma (SaOS-2) cells," *Acta Metallurgica Sinica*, vol. 27, no. 6, pp. 1152–1158, 2014.

[37] E. Cremonini, E. Zonaro, M. Donini et al., "Biogenic selenium nanoparticles: characterization, antimicrobial activity and effects on human dendritic cells and fibroblasts," *Microbial Biotechnology*, vol. 9, no. 6, pp. 758–771, 2016.

[38] M. J. Masarudin, S. M. Cutts, B. J. Evison, D. R. Phillips, and P. J. Pigram, "Factors determining the stability, size distribution, and cellular accumulation of small, monodisperse chitosan nanoparticles as candidate vectors for anticancer drug delivery: application to the passive encapsulation of [14C]-doxorubicin," *Nanotechnology, Science and Applications*, vol. 8, p. 67, 2015.

[39] A. V. Tugarova and A. A. Kamnev, "Proteins in microbial synthesis of selenium nanoparticles," *Talanta*, vol. 174, pp. 539–547, 2017.

[40] S. R, M. M, and V. N. Yogananda Murthy, "Biosynthesis and characterization, antioxidant and antimicrobial activities of selenium nanoparticles from ethanol extract of bee propolis," *Journal of Nanomedicine & Nanotechnology*, vol. 10, no. 01, 2019.

[41] S. N. Borah, L. Goswami, S. Sen et al., "Selenite bioreduction and biosynthesis of selenium nanoparticles by Bacillus paramycoides SP3 isolated from coal mine overburden leachate," *Environmental Pollution*, vol. 285, Article ID 117519, 2021.

[42] A. J. Kora and L. Rastogi, "Peroxidase activity of biogenic platinum nanoparticles: a colorimetric probe towards selective detection of mercuric ions in water samples," *Sensors and Actuators B: Chemical*, vol. 254, pp. 690–700, 2018.